Earth and Planetary Science Letters 394 (2014) 198–208

Contents lists available at ScienceDirect

Earth and Planetary Science Letters

www.elsevier.com/locate/epsl

Distinct roles of the Southern Ocean and North Atlantic in the deglacial atmospheric radiocarbon decline

Mathis P. Hain [a,b,*], Daniel M. Sigman [a], Gerald H. Haug [c]

[a] Princeton University, Department of Geosciences, Guyot Hall, Princeton, NJ 08544, USA
[b] National Oceanography Centre Southampton, University of Southampton, SO14 3ZH, UK
[c] ETH Zürich, Geological Institute, Department of Earth Sciences, Sonneggstrasse 5, Zürich 8092, Switzerland

ARTICLE INFO

Article history:
Received 20 May 2013
Received in revised form 5 March 2014
Accepted 10 March 2014
Available online xxxx
Editor: J. Lynch-Stieglitz

Keywords:
deglaciation
ice age
carbon cycle
radiocarbon
ocean circulation
AMOC

ABSTRACT

In the context of the atmospheric CO_2 $^{14}C/C$ ($\Delta^{14}C_{atm}$) changes since the last ice age, two episodes of sharp $\Delta^{14}C_{atm}$ decline have been related to either the venting of deeply sequestered low-^{14}C CO_2 through the Southern Ocean surface or the abrupt onset of North Atlantic Deep Water (NADW) formation. In model simulations using an improved reconstruction of ^{14}C production, Atlantic circulation change and Southern Ocean CO_2 release both contribute to the overall deglacial $\Delta^{14}C_{atm}$ decline, but only the onset of NADW can reproduce the sharp $\Delta^{14}C_{atm}$ declines. To fully simulate $\Delta^{14}C_{atm}$ data requires an additional process that immediately precedes the onsets of NADW. We hypothesize that these "early" $\Delta^{14}C_{atm}$ declines record the thickening of the ocean's thermocline in response to reconstructed transient shutdown of NADW and/or changes in the southern hemisphere westerly winds. Such thermocline thickening may have played a role in triggering the NADW onsets.

1. Introduction

Atmospheric $^{14}C/C$ has declined from the Last Glacial Maximum (LGM) to the preindustrial modern, with two main episodes of rapid $\Delta^{14}C_{atm}$ decline during deglaciation (e.g., Hughen et al., 2004; Bronk Ramsey et al., 2012; Southon et al., 2012) (Fig. 1). The significance of this record is vigorously debated. Two explanations have been proposed for the sharpest $\Delta^{14}C_{atm}$ declines: (a) the Southern Ocean ventilation of an hypothesized isolated volume of carbon dioxide-rich abyssal water, yielding synchronous atmospheric CO_2 rise and $\Delta^{14}C_{atm}$ decline (Broecker and Barker, 2007; Marchitto et al., 2007; Skinner et al., 2010), or (b) the resumption of NADW formation transferring ^{14}C from the atmosphere into the deep ocean (Keir, 1983; Hughen et al., 1998, 2004; Köhler et al., 2006; Laj et al., 2004; Muscheler et al., 2008), in which case $\Delta^{14}C_{atm}$ is expected to decline most steeply only after most of the atmospheric CO_2 rise. In general, however, skepticism has been expressed that any oceanic mechanism can explain the observed $\Delta^{14}C_{atm}$ changes (Broecker, 2009).

Here, supported by an improved estimate of ^{14}C production rate change, we attempt a complete simulation of the deglacial $\Delta^{14}C_{atm}$ history. We find that the $\Delta^{14}C_{atm}$ history is surprisingly consistent with the consensus view of deglacial ocean changes, with alternating increases in North Atlantic deep ventilation and Southern Ocean CO_2 release. Two subtle but coherent deviations between model and observations that immediately precede the onsets of NADW formation at ~12 and ~15 thousand years before present (kyr BP) can be taken as evidence for one further ingredient, and we will argue that this as-of-yet unrecognized dynamic may be important in the mechanism of the South-to-North teleconnection.

2. Methods

2.1. The new CYCLOPS model

All carbon cycle model simulations in this study were generated using a new high-performance implementation of the legacy CYCLOPS global carbon cycle box model (e.g., Hain et al., 2010; Keir, 1988; Sigman et al., 1998, 2003; Robinson et al., 2005b). We use the same model configuration as in (Hain et al., 2010, 2011), with 18 ocean reservoirs, one atmospheric carbon reservoir, and one fixed size terrestrial carbon reservoir (3000 PgC). The operation of the biological carbon pumps is simulated as in (Hain et al., 2010). The lysocline model controlling the open system $CaCO_3$ cycle is a combination of the "rain-based" version of seafloor $CaCO_3$ model of (Sigman et al., 1998), the bottom water under-saturation driven part of the (Archer, 1991) $CaCO_3$ diagenesis model, and net-throughput sediment mixed layer model with

* Corresponding author at: National Oceanography Centre Southampton, University of Southampton, SO14 3ZH, UK.
E-mail address: m.p.hain@soton.ac.uk (M.P. Hain).

http://dx.doi.org/10.1016/j.epsl.2014.03.020
0012-821X/

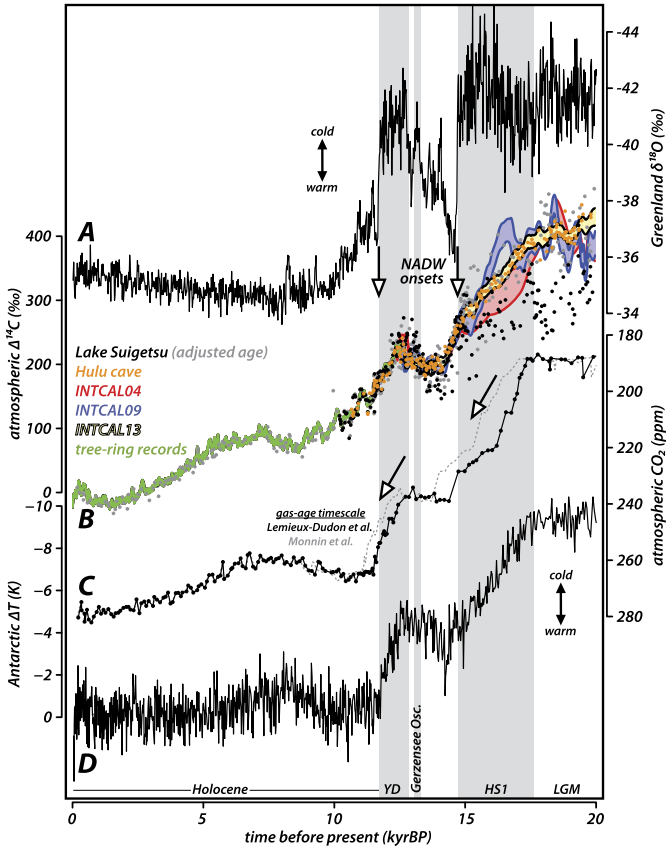

Fig. 1. Records of deglacial changes in climate and the carbon cycle. (A) Greenland (NGRIP) ice core $\delta^{18}O$ on GICC timescale (Andersen et al., 2006; NGRIP members, 2004; Rasmussen et al., 2006; Vinther et al., 2006). (B) Atmospheric $\Delta^{14}C$ ($\Delta^{14}C_{atm}$) datasets (Bronk Ramsey et al., 2012; Southon et al., 2012; Reimer et al., 2009, 2004, 2013). (C) Reconstructed atmospheric CO_2 levels (gray dashed: Monnin et al., 2001) on revised timescale (black: Lemieux-Dudon et al., 2010). (D) Antarctic temperature changes (Jouzel et al., 2007). The driving mechanisms for rapid $\Delta^{14}C_{atm}$ decline ~12 and ~15 kyrs BP are debated, with ocean CO_2 release and North Atlantic circulation changes as the main contending explanations.

millennial adjustment timescale for percent $CaCO_3$ on the seafloor (see Supplementary Information).

2.2. Sensitivity experiments

In this study, we consider the effect of six distinct mechanisms that are linked to deglacial changes in ocean circulation and biogeochemistry (reviewed by Hain et al., 2014): (#1) Polar Antarctic stratification during the LGM, with subsequent destratification (e.g., François et al., 1997; Sigman et al., 2010); (#2) glacial expansion and deglacial retreat of Southern Ocean sea ice (e.g., Collins et al., 2012; Stephens and Keeling, 2000); (#3) the deglacial rise of Polar Antarctic preformed nutrient concentration (François et al., 1997; Robinson et al., 2004; Robinson and Sigman, 2008); (#4) the rapid end of enhanced iron fertilization in the Subantarctic (Kohfeld et al., 2005; Kumar et al., 1995; Martin, 1990; Martinez-Garcia et al., 2009) that led to a rise in surface nutrient concentration (Robinson et al., 2005b; Martinez-Garcia et al., 2014); (#5) the stalling of Atlantic meridional overturning associated with Heinrich Stadial 1 (HS1) and the Younger Dryas (YD) (e.g., Lippold et al., 2012; McManus et al., 2004; Robinson et al., 2005a); and (#6) the abrupt resumption of North Atlantic Deep Water formation at the onsets of the Bølling/Allerød interstadial and the Holocene interglacial (e.g., McManus et al., 2004; Ritz et al., 2013; Robinson et al., 2005a). Additionally, we test for the impact of deepening/thickening of the ocean's main thermocline, which we will argue below caused $\Delta^{14}C_{atm}$ decline just prior to NADW resumption at the end of HS1 and YD.

All transient sensitivity experiments are initialized with the steady state LGM carbon cycle scenario of (Hain et al., 2010, 2011), to which we have increased sea ice cover in the Antarctic, reducing the surface area available for gas-exchange of the Polar Antarctic Zone (PAZ) box by 50%. From this starting point, individual Southern Ocean-related model parameters (#1–4) were abruptly reverted to their respective interglacial model reference values. For the North Atlantic circulation changes, we test both the abrupt transition from GNAIW-circulation to (#5) HS-circulation and to (#6) NADW-circulation (Fig. S1). All individual sensitivity experiments and their outcomes are described in detail in the Supplementary Information and listed in Table S1 for 1, 5 and 60 thousand years after the abrupt forcing. For brevity, Section 3.1 describes only the 1 kyr sensitivities and conflates the Polar Antarctic Zone experiments (#1–3).

The use of "GNAIW" circulation for the LGM (instead of the IG reference "NADW" circulation) directly relates to the finding of a mid-depth Atlantic $\delta^{13}C$ gradient during the LGM, which implies shoaling of the depth to which the ice age North Atlantic ventilated the ocean interior (e.g., Duplessy et al., 1988; Curry and Oppo, 2005; Marchitto and Broecker, 2006; see review by Lynch-Stieglitz et al., 2007). It also relates to the very high $\delta^{13}C$ and low nutrient concentration of northern-sourced water during the LGM (Marchitto et al., 1998), the combination of which is difficult to simulate without allowing the downstream advection of North Atlantic-sourced mid-depth water to extend beyond the Atlantic basin (Sigman et al., 2003). We note that, in the GNAIW circulation scheme (Sigman et al., 2003), wind-driven upwelling in the open Antarctic returns mid-depth water (instead of deep water, as in the NADW scheme) to the surface so as to balance the formation of intermediate-depth rather than deep water in the North Atlantic (Fig. S1).

2.3. ^{14}C production and global budget

The global budget of ^{14}C and the abundance of ^{14}C on the planet during the deglaciation are a function of the time-variant rate of cosmogenic ^{14}C production and the regular radioactive decay of this isotope (with a half-life of 5730 yr). Cosmogenic ^{14}C production is affected by the strength of Earth's magnetic field, which shields the atmosphere from high energy cosmic particles, and the solar modulation of the incidence of high energy cosmic particles (Lal and Peters, 1967).

To calculate the global budget of ^{14}C, we extend and update the approach of Hughen et al. (2004), Köhler et al. (2006) and Laj et al. (2002, 2004):

(1) The GLOPIS-75 reconstruction of Earth's magnetic field strength of the last 75 thousand years ago and the associated uncertainty envelope (Laj et al., 2004) are used with linear interpolation (Fig. 2A).
(2) Using a recent model of cosmogenic production of ^{14}C (Kovaltsov et al., 2012), global ^{14}C production (Fig. 2B) is calculated as a function of the time-variant GLOPIS-75 field strength (M) and a constant solar modulation potential (Φ = 550 MV; see also Bard, 1998). Using the Kovaltsov et al. (2012) model, we calculate a modern ^{14}C production rate of ~1.8 atom cm^{-2} s^{-1} (Fig. 2B), a preindustrial bulk global decay rate of ~1.7 dps cm^{-2} (Fig. 2C), and a global bulk $\Delta^{14}C$ of −110‰ (Fig. 2D), which is in good agreement with the $\Delta^{14}C$ of the ocean carbon pool. As pointed out by Kovaltsov et al. (2012), earlier models (e.g., 2.05 atom cm^{-2} s^{-1}, Masarik and Beer, 2009) overestimated global ^{14}C production due to outdated cosmic ray spectra used in the calculations.

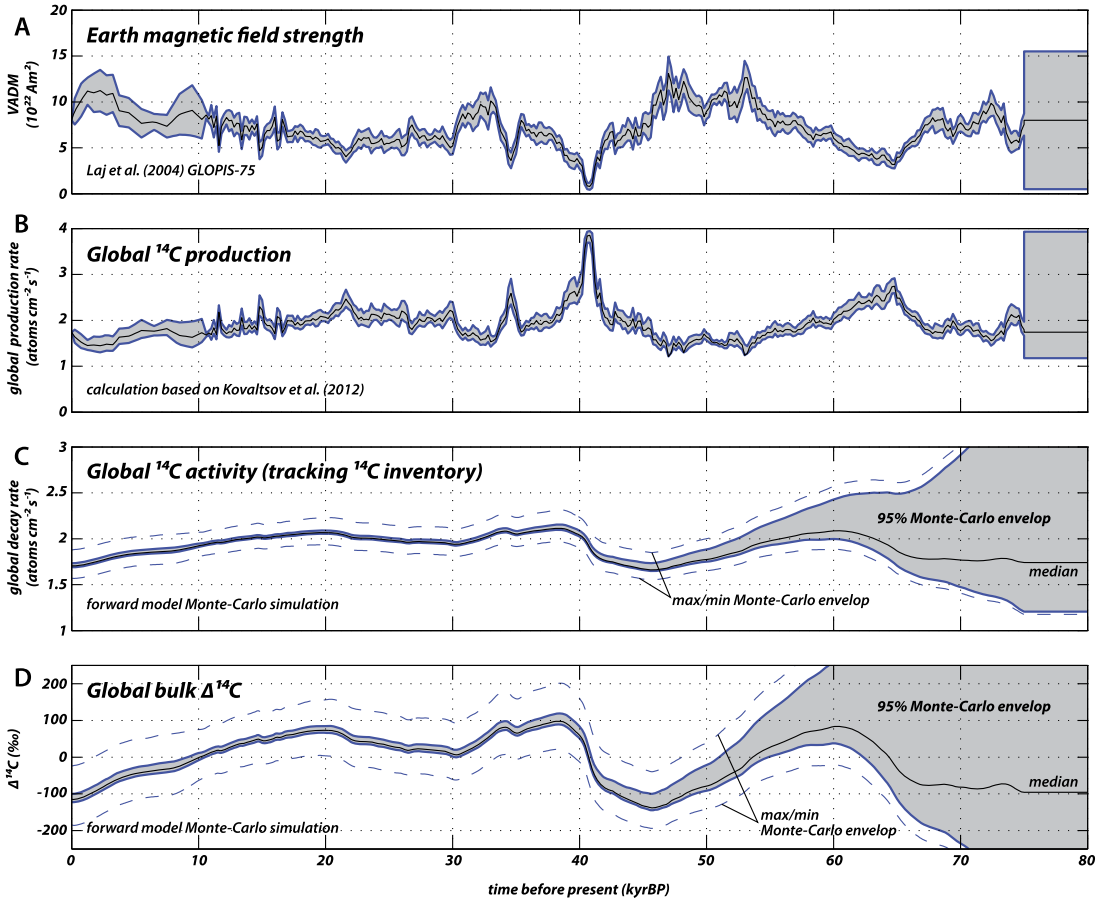

Fig. 2. Deglacial ^{14}C budget based on magnetic field strength changes. (A) GLOPIS-75 paleomagnetic reconstruction (Laj et al., 2004). (B) ^{14}C production history calculated using the model of Kovaltsov et al. (2012). (C) Global inventory of ^{14}C shown as activity (i.e., ^{14}C decays per second per square centimeter of Earth surface). (D) Global bulk $\Delta^{14}C$ calculated based on the time variant ^{14}C inventory and a constant 43,000 PgC inventory of stable carbon isotopes ($\delta^{13}C = 0‰$ *versus* PDB).

(3) To propagate the uncertainty of the GLOPIS-75 record, we construct a Monte-Carlo simulation with 1000 members of randomized magnetic field strength records, all of which fall within and span the GLOPIS-75 uncertainty envelope (Fig. 2A). To be conservative, we use a uniform distribution (rather than a normal distribution) to represent the GLOPIS-75 uncertainty. The calculated ^{14}C production (Fig. 2B) can be integrated through time to calculate the planetary ^{14}C inventory through time (Fig. 2C) and the expected isotopic composition ($\Delta^{14}C$) of a global inventory of 43,000 PgC in the climate system (Fig. 2D). The vast majority (95%) of the Monte-Carlo member scenarios fall within a very narrow band (gray in Figs. 2C and 2D), which is embedded within a wider band that includes all values produced by individual Monte-Carlo ensemble members (dashed lines in Figs. 2C and 2D). The same Monte-Carlo ensemble is used throughout the manuscript, and the 95% uncertainty envelope is shown for the carbon cycle model results.

To our knowledge, this is the first calculated global ^{14}C budget that correctly predicts (within uncertainty) the ^{14}C content of the preindustrial ocean/atmosphere/biosphere carbon reservoir, while previous calculations using the cosmogenic ^{14}C production model of Masarik and Beer (1999) (i.e., scaling ^{14}C production to a modern ^{14}C production rate of 2.02 atom cm^{-2} s^{-1}) yielded greater predicted global ^{14}C activity than can be accounted for by the major exchanging carbon reservoirs of the climate system (see supplementary information in Hughen et al., 2004). This lends support to the combined use of GLOPIS-75 magnetic field strength record (Laj et al., 2004) and the Kovaltsov et al. (2012) model for cosmogenic ^{14}C production to calculate the deglacial global ^{14}C budget. The calculated ^{14}C production history, global ^{14}C inventory through time, and bulk global $\Delta^{14}C$ through time are appended online in tabulated form (see Supplementary Information).

2.4. Deglacial experiments

2.4.1. Deep ventilation by the North Atlantic and Southern Ocean

To simulate the effect of deglacial ocean and carbon cycle changes on atmospheric $\Delta^{14}C$, we use three idealized time-transient model forcings that change the conditions in (1) the Polar Antarctic Zone (PAZ box), (2) the Subantarctic Zone of the Southern Ocean (SAZ box), and (3) North Atlantic overturning and its downstream advective circulation (Fig. 3; additional description in Supplementary Information). The timing of these changes is based on the NGRIP ice core chronology (Rasmussen et al., 2006).

While some details of these time-transient changes can and should be questioned, we believe these forcings capture the essence of the consensus view of deglaciation – with the exception of the Gerzensee Oscillation being incorporated into the Younger Dryas stage of stalled North Atlantic overturning. We believe that the last is justifiable for 4 reasons. First, the Gerzensee Oscillation has long been identified as a period of circum-North Atlantic cooling (Eicher and Siegenthaler, 1976; Lehman and Keigwin, 1992; Levesque et al., 1993; Andresen et al., 2000), with the caveat that different terminologies are used for central Europe (Gerzensee Oscillation), North America (Killarney Oscillation), North Atlantic (Intra-Allerød Cold Period, IACP), and Greenland (Greenland Interstadial stage 1b, GI-1b). Second, evidence for catastrophic drainage

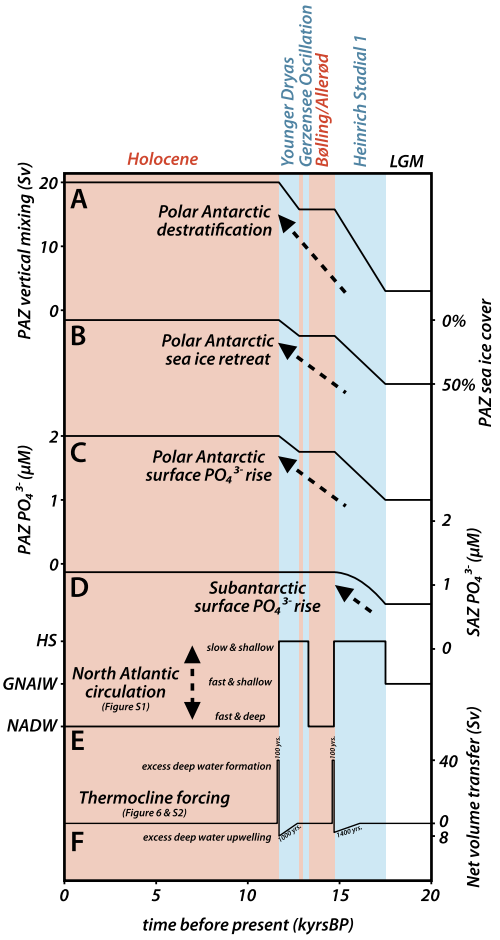

Fig. 3. Model forcings used for time-dependent deglacial simulations in Figs. 5 and 6. (A) Vertical exchange between the Polar Antarctic Zone (PAZ) and Circumpolar Deep Water boxes. (B) PAZ sea ice cover, in percent of box surface area. (C) PAZ surface PO_4^{3-} concentration. (D) Subantarctic Zone (SAZ) box surface PO_4^{3-} concentration. (E) North Atlantic circulation switches between "GNAIW", "HS" and "NADW" model circulation schemes (Fig. S1). (F) Use of an unbalanced "transfer" circulation (Fig. S2) that repartitions ocean volume between deep and mid-depth model boxes.

of the Glacial Lake Iroquois at the onset of the Gerzensee Oscillation has been invoked as a trigger for a reduction in Atlantic overturning (Donnelly et al., 2005). Third, as with HS1 and the Younger Dryas, the Gerzensee Oscillation has a clear effect on the East Asian Monsoon (Wang et al., 2001) and atmospheric methane (Blunier and Brook, 2001). Fourth, based on the high resolution age model of van Raden et al. (2013), only 112 yr of latest Allerød warmth separate the ~300 yr long Gerzensee Oscillation (13 274 to 12 989 yr BP) from the beginning transition (12 877 yr BP) towards cold Younger Dryas Stadial climate, making the distinction between Younger Dryas and Gerzensee Oscillation difficult to resolve in marine records.

2.4.2. Thermocline volume

Forced changes in the thermocline volume are driven by two opposing unbalanced "transfer" circulation schemes that do not conserve the volume of individual ocean boxes: (a) unbalanced Ekman transport from the deep ocean to the mid-depth ocean across the open Antarctic and Subantarctic boxes (blue in Fig. S2), and (b) excess formation of NADW that transfers volume from the mid-depth boxes via the deep North Atlantic back to the global deep ocean (red in Fig. S2). These transfer circulations repartition ocean volume (i.e., water and its dissolved chemicals) between boxes. This is in contrast to the model's other circulation schemes, which are balanced so as not to cause box volume changes. All circulations schemes conserve total ocean volume and inventory of chemicals.

To simulate changes in thermocline volume associated with the HS1/Bølling transition, we couple the two transfer circulations as follows (Fig. 3F). First, a linear increase in the Ekman transfer circulation over the course of the final 1400 yr of the HS1 stalling of North Atlantic overturning is used to simulate a "wind-driven" thickening of the global thermocline. Second, upon the HS1/Bølling transition, we use the excess NADW transfer circulation at 40 Sv for the duration of 100 yr so as to transfer the volume back from the thermocline to the deep ocean. Thermocline changes associated with the YD/Holocene transition are simulated in the same way, but "wind-driven" Ekman transfer is ramped-up more steeply and over a period of only 1000 yr (yielding the same cumulative volume transfer). For both HS1/Bølling and YD/Holocene transitions, cumulative wind-driven upwelling equals cumulative excess NADW formation such that, after each of the two forcing couplets (Ekman transfer followed by excess NADW transfer), the distribution of box volumes is restored to the model's reference configuration. This simulated change in thermocline thickness is well-founded at a mechanistic level, as discussed below (Section 4): a thickening/deepening of the main pycnocline of the global ocean is expected from continued (and possibly strengthened) wind-driven upwelling in the absence of North Atlantic Deep Water formation. However, there is a general lack of observations that speak to its occurrence and timing, and the datasets that could be argued to support thermocline deepening (e.g., Siani et al., 2013) have not been interpreted in that way. In this context, this model exercise should not be understood as a process estimate but rather as a first exploration of the sensitivity of $\Delta^{14}C_{atm}$ to a thickening/deepening of the main pycnocline of the global ocean.

3. Results

3.1. CO_2 versus $\Delta^{14}C_{atm}$ sensitivities

Our knowledge of the global ocean circulation and air/sea carbon exchange predicts distinct radiocarbon and CO_2 effects of deep ocean ventilation by the North Atlantic and the Southern Ocean (Fig. 4). To clarify these expectations and the principle dynamics, we focus here on the results of five 1000-yr sensitivity experiments: (1) transition of North Atlantic-sourced overturning from GNAIW- to NADW-based, (2) stalling of GNAIW-based overturning, (3) demise of glacial Subantarctic Zone iron fertilization, (4) combined Polar Antarctic Zone destratification, sea ice retreat and rise of unused surface nutrients, and (5) a 100 m thickening of the global thermocline as a result of 1 Sv excess upwelling. Detailed analysis of all seven tested mechanisms is provided in the Supplementary Information (Text S4, Table S1).

First, the circulation of the LGM scenario is replaced with the model's modern reference "NADW" circulation (red arrow in Fig. 4B), which includes direct advection from the North Atlantic into the deep ocean instead of into the mid-depth ocean as in the glacial "GNAIW" circulation. This deepening of North Atlantic circulation (GNAIW to NADW) acts to reduce $\Delta^{14}C_{atm}$ by ~83‰ because well-equilibrated (high-$\Delta^{14}C$) North Atlantic surface water displaces low-$\Delta^{14}C$ southern sourced water at depth. In the complementary second experiment (blue arrow in Fig. 4B), the GNAIW of the LGM scenario is replaced by a Heinrich Stadial "HS" circulation state with no North Atlantic advective overturning, which acts to raise $\Delta^{14}C_{atm}$ by 63‰. These estimates are in general agreement with previous sensitivity studies for the effect of North Atlantic circulation on $\Delta^{14}C_{atm}$ (Hughen et al., 1998; Köhler et al., 2006; Laj et al., 2004; Muscheler et al., 2008; but see also Matsumoto and Yokoyama, 2013). The weakness of the CO_2 changes in the North Atlantic circulation experiments is largely due

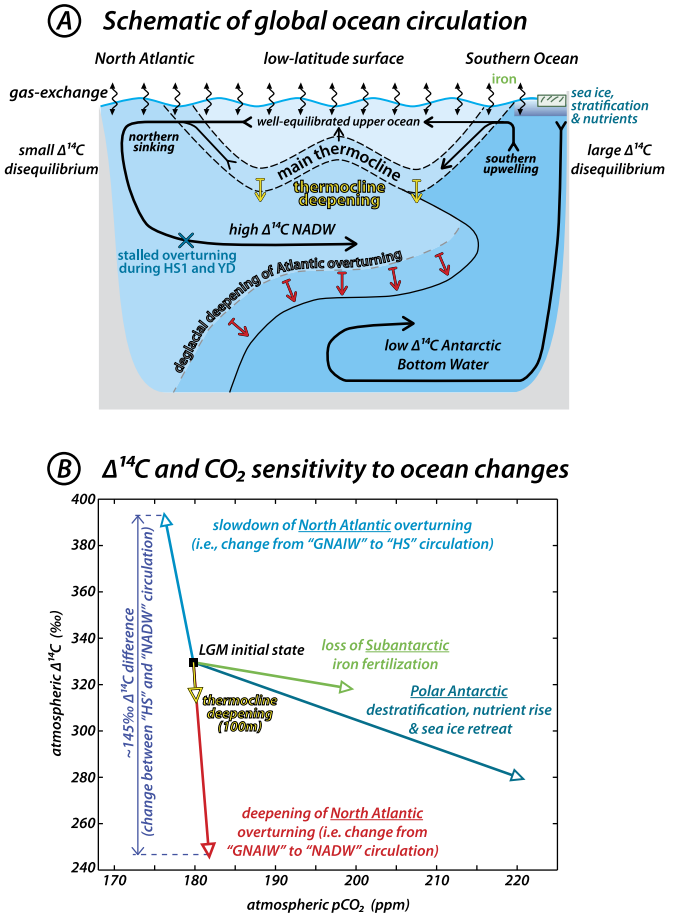

Fig. 4. Mechanisms for altering ocean/atmosphere CO_2 and ^{14}C partitioning explored in this study, schematically (A) and by modeled sensitivities (B). (A) Gas exchange and ocean circulation that lead to ^{14}C uptake by the ocean (black arrows), with mechanisms for deglacial change illustrated by colored arrows/text. $\Delta^{14}C$-equilibration occurs through gross gas exchange that scales with ocean surface area, such that the aerially-limited polar oceans tend to be poorly equilibrated with $\Delta^{14}C_{atm}$. North Atlantic Deep Water (NADW) formation, however, is partially fed by well-equilibrated low-latitude surface water, thereby making North Atlantic-sourced waters a dominant vector for ^{14}C partitioning from the atmosphere into the deep ocean interior. An excess of wind-driven "southern upwelling" over "northern sinking" implies that buoyant water accumulates in the upper ocean so as to deepen the ocean's main thermocline. (B) Sensitivities of $\Delta^{14}C_{atm}$ and CO_2 to deglacial mechanisms as derived from 1000-yr transient model simulations (see also Suppl. Inf. and Table S1). Arrow and text colors follow those of the mechanisms labeled in (A). (The full-color figure does not appear in print, and the reader is referred to the digital version of this article.)

to counteracting effects (Hain et al., 2010, 2014; Kwon et al., 2011, 2012): NADW formation strengthens the ocean's biological pump by filling the interior with water low in preformed nutrients, but it decreases ocean alkalinity by driving a $CaCO_3$ preservation event in the deep sea.

The third and fourth sensitivity experiments simulate Southern Ocean changes that increase atmospheric CO_2 significantly, and their CO_2 effects are still greater on a longer (~5 kyr) time scale. However, they yield only modest changes in $\Delta^{14}C_{atm}$ (green and teal blue arrows in Fig. 4B). This weak sensitivity of $\Delta^{14}C_{atm}$ to Southern Ocean surface conditions, as compared to their substantial effect on atmospheric CO_2, relates to the long equilibration timescale of $\Delta^{14}C$. While CO_2 release from surface waters results from net carbon transfer that occurs on a timescale of months, carbon isotopic equilibration by gross exchange of CO_2 molecules operates on a timescale of years (Lynch-Stieglitz et al., 1995). Since the relatively small area of the polar Southern Ocean limits gross CO_2 exchange, the Southern Ocean surface and newly forming deep water retains substantial $\Delta^{14}C$ disequilibrium and thus a high apparent ^{14}C age (Fig. 4A; Southern Ocean loop). The slow equilibration of $\Delta^{14}C$ sets up a trade-off in which deglacial destratification around Antarctica reduces the true ventilation age of the deep ocean but also acts to raise the apparent age of descending Antarctic surface water, which reduces its overall effect on the partitioning of ^{14}C between atmosphere and ocean as reflected in the apparent ^{14}C age of the deep ocean. In contrast, NADW is partly derived from low-latitude surface water that is well equilibrated with $\Delta^{14}C_{atm}$ due its lengthy residence in the vast area of the low-latitude ocean (Fig. 4A; North Atlantic loop). Thus, in the modern ocean, NADW is a principle vector for the partitioning of ^{14}C from the atmosphere into the ocean, and the initiation of NADW formation during deglaciation should have led to substantial decline in $\Delta^{14}C_{atm}$ (Hughen et al., 1998; Köhler et al., 2006; Laj et al., 2004; Muscheler et al., 2008; Robinson et al., 2005a).

The fifth sensitivity experiment simulates a deepening of the ocean's main thermocline arising from an imbalance between "southern upwelling" and "northern sinking" (Fig. 4A; e.g., Gnanadesikan, 1999). A transient imbalance leading to a deepening in the thermocline would seem likely during HS1 and YD, when NADW/GNAIW formation was minimal and Antarctic upwelling continued and has been proposed to have strengthened (e.g., Anderson et al., 2009; Denton et al., 2010). As described below, a deepening of the thermocline is also of interest for its potential physical role in the onset of vigorous North Atlantic Deep Water formation at the Bølling and after the YD.

The warm, buoyant, low latitude upper ocean accounts for a modest fraction of the ocean's volume but the vast majority of the ocean's surface area, such that these waters are near $\Delta^{14}C$ equilibrium with the atmosphere (Hain et al., 2011). The $\Delta^{14}C$ of the atmosphere and of the upper ocean must decline as the thermocline deepens and the volumetric importance of the upper ocean rises at the expense of the ^{14}C-depleted deep ocean interior. Our model predicts a ~13‰ $\Delta^{14}C_{atm}$ decline per 100 m of thermocline deepening (Fig. 4B).

3.2. Deglacial simulations

3.2.1. ^{14}C production rate change

A large portion of the atmospheric $\Delta^{14}C$ decline since the last ice age was due to a deglacial strengthening of Earth's magnetic field that more effectively shielded the atmosphere from cosmogenic ^{14}C production (Fig. 2) (Laj et al., 2002, 2004). Specifically, our ^{14}C budget suggests a global ^{14}C activity of ~2.1 decays per second per square centimeter (of Earth's surface) during the LGM compared to ~1.7 before nuclear activities (Fig. 2C). Given the ~43,000 Pg carbon in the climate system, this change in ^{14}C inventory suggest that bulk $\Delta^{14}C$ declined from about 80‰ to about −120‰ across deglaciation (Fig. 2D), accounting for roughly half of the reconstructed deglacial $\Delta^{14}C_{atm}$ change (Fig. 5A).

The GLOPIS-75 magnetic field strength dataset (Laj et al., 2004) exhibits a number of large, short-term negative excursions between 17 kyr BP and 10 kyr BP, for which the dataset is based on marine sediment magnetization. These spikes may be artifacts (e.g., Valet, 2003). Taking the GLOPIS-75 dataset at face value and including the spikes has very limited effect on the global ^{14}C inventory (Figs. 2C and D) because the spikes cause relatively little "extra" ^{14}C when compared to all ^{14}C on Earth. However, the brief pulses of "extra" ^{14}C transiently augment the ^{14}C in the atmosphere before they are spread through the ocean and land carbon reservoirs (see Fig. 5A).

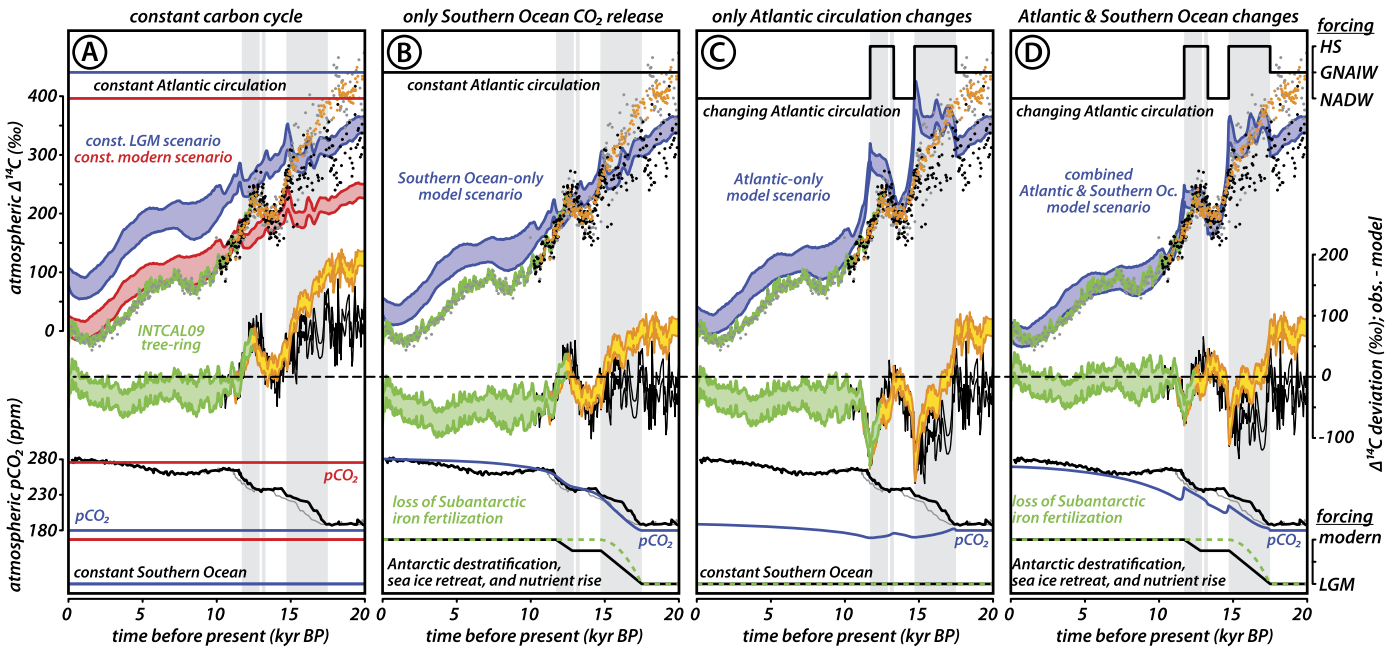

Fig. 5. Model output for the different deglacial scenarios compared to data on atmospheric radiocarbon (black/gray: Bronk Ramsey et al., 2012; orange: Southon et al., 2012; green: tree-ring data aggregated by Reimer et al., 2009) and CO_2 (gray dashed: Monnin et al., 2001; black: timescale of Lemieux-Dudon et al., 2010). Scenarios: (A) constant LGM (blue) and Holocene (red) carbon cycle, (B) Southern Ocean deglacial forcing only, (C) North Atlantic circulation changes only, and (D) combined Southern Ocean and North Atlantic deglacial forcing. Each scenario consists of 1000 simulations that capture the uncertainty of the ^{14}C-production history (see Fig. 2). The forcings are described in Section 2.4.1 and Fig. 3. Notably, Southern Ocean changes dominate simulated deglacial CO_2 rise, whereas all changes contribute to $\Delta^{14}C_{atm}$ decline, and North Atlantic circulation changes cause abrupt shifts in simulated $\Delta^{14}C_{atm}$. (The full-color figure does not appear in print, and the reader is referred to the digital version of this article.)

3.2.2. Southern Ocean and North Atlantic deglacial changes

In the first set of deglacial experiments (Fig. 5A), the $\Delta^{14}C_{atm}$ history is simulated assuming constant states for the carbon cycle and ocean circulation, for two cases: the interglacial reference case (red) and our LGM scenario (blue). Next, the deglacial Southern Ocean experiments are applied (Fig. 5B). As the main point of comparison, we conduct an experiment of only North Atlantic circulation changes (Fig. 5C), in which the transition from GNAIW in the LGM to NADW in the Holocene is interrupted by two episodes of stalled North Atlantic overturning. Finally, we combine these time-dependent Southern Ocean and North Atlantic changes (Fig. 5D) to assess their combined effect on $\Delta^{14}C_{atm}$ relative to observations.

The simulations are compared to terrestrial records of $\Delta^{14}C_{atm}$ based on (a) the well-constrained tree-ring record back to 12.4 thousand years ago (green; Friedrich et al., 2004; Reimer et al., 2009 and references therein), (b) varved sediments from Lake Suigetsu in Japan, which are shown according to two different age models for the sediments (black/gray; Bronk Ramsey et al., 2012), and (c) "dead carbon fraction"-corrected data from the U–Th series dated Hulu Cave (orange; Southon et al., 2012).

During deglaciation, the $\Delta^{14}C_{atm}$ data appear to switch repeatedly between the $\Delta^{14}C_{atm}$ histories predicted for the constant LGM and Holocene scenarios (blue and red in Fig. 5A). To the degree that the global ^{14}C budget presented here is accurate, the difference between observed $\Delta^{14}C_{atm}$ and the constant Holocene carbon cycle model scenario (red in Fig. 5A) indicates past differences in ocean circulation and the carbon cycle from interglacial conditions. Positive differences between observed and simulated $\Delta^{14}C_{atm}$ occur at around 12.5 and prior to ~15 thousand years ago (black and orange envelopes in Fig. 5A relative to varve counted Lake Suigetsu and Hulu Cave records, respectively), and there is a slight negative deviation over the last 10 thousand years (light green envelope in Fig. 5A relative to tree-ring record).

In the simulation of changing Southern Ocean conditions (Fig. 5B), increased overturning in the polar Southern Ocean causes the deep ocean ^{14}C ventilation age to decline. In addition, retreating Southern Ocean sea ice enlarges the polar surface area available for isotopic equilibration, thereby driving a net transfer of ^{14}C from the atmosphere to the deep ocean. Finally, the net release of CO_2 from the deep ocean to the atmosphere drives a global increase in gross air–sea CO_2 exchange, causing a global decrease in surface reservoir ages (Bard, 1998 and references therein). All three changes combined drive 50‰ to 60‰ of simulated $\Delta^{14}C_{atm}$ decline over the entire deglaciation, with 45‰ of the decline occurring gradually over the course of HS1 (Fig. 6E). Simulated atmospheric CO_2 rise and $\Delta^{14}C_{atm}$ decline are synchronous, as predicted by Southern Ocean explanations for deglacial $\Delta^{14}C_{atm}$ decline (Skinner et al., 2010). However, even when taken together, the Southern Ocean changes are insufficient to explain the magnitude and rate of $\Delta^{14}C_{atm}$ decline associated with HS1 and YD.

In the simulation of changing only North Atlantic circulation (Fig. 5C), switching from GNAIW during the LGM to NADW during the Holocene causes a net $\Delta^{14}C_{atm}$ decline of 60‰ to 75‰, which is similar to but greater than the net effect of Southern Ocean CO_2 release (Fig. 6E). The transitions from HS to NADW circulation at the HS1/Bølling and the YD/Holocene boundaries cause two episodes of abrupt ~125‰ decline in $\Delta^{14}C_{atm}$ (Fig. 5C). Thus, the North Atlantic circulation forcing imposes substantial dynamic variability on simulated $\Delta^{14}C_{atm}$, while the transition from GNAIW to NADW is the dominant single contributor to net deglacial $\Delta^{14}C_{atm}$ decline, aside from ^{14}C production rate decline.

The $\Delta^{14}C_{atm}$ effects of the North Atlantic and Southern Ocean forcings are roughly additive, together yielding a contribution of 80‰ to 110‰ to net deglacial $\Delta^{14}C_{atm}$ decline (Fig. 5D). Southern Ocean CO_2 release causes synchronous $\Delta^{14}C_{atm}$ decline during times of stalled North Atlantic circulation, and the resumption of NADW drives rapid $\Delta^{14}C_{atm}$ decline that lags rising CO_2. The combination of our global ^{14}C budget, Southern Ocean CO_2 release and North Atlantic circulation changes yields a simulated

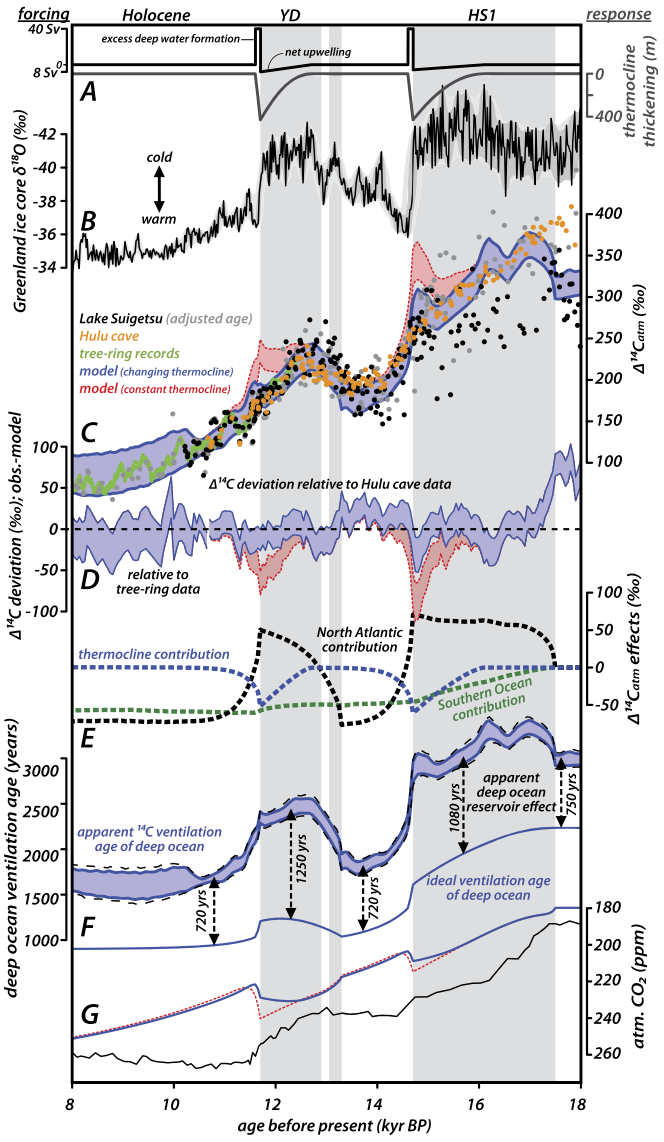

Fig. 6. Speculative deglacial scenario with wind-driven thickening of the global thermocline (blue) compared to baseline deglacial scenario of Fig. 5D (red dashed). (A) Forced net transfer of water (black) from the deep into the upper ocean by enhanced Ekman transport (net upwelling) thickens the global thermocline (gray line), which is reversed by short pulses of excess deep water formation. (B) NGRIP $\delta^{18}O$ motivates the imposed timing of NADW changes (Figs. 3E and 5C; Anderson et al., 2006; NGRIP members 2004; Rasmussen et al., 2006; Vinther et al., 2006). (C) Reconstructed $\Delta^{14}C_{atm}$ (Bronk Ramsey et al., 2012; Southon et al., 2012; tree-ring data aggregated by Reimer et al., 2009) is closely matched by the revised scenario (blue), whereas (D) the baseline scenario (red dashed) deviates from these data during two well-defined episodes. (E) Diagnosis of the distinct effects on $\Delta^{14}C_{atm}$ imposed by Southern Ocean, North Atlantic and thermocline forcings demonstrates that Atlantic circulation changes are responsible for the sharp transitions in simulated $\Delta^{14}C_{atm}$. (F) The age of bulk deep ocean ventilation illustrates that changes in ocean ventilation rate (ideal ventilation age) and the state of surface ^{14}C-equilibration (reservoir effect) contribute to simulated air/sea ^{14}C partitioning. (G) Atmospheric CO_2 for the deglacial scenario with (blue) and without (red) simulated thermocline deepening, compared to data (black; Monnin et al., 2001; Lemieux-Dudon et al., 2010). The disagreement between simulated and reconstructed CO_2 may be due to the lack of simulated ocean warming and/or the timescale of ocean alkalinity loss, neither of which have significant effect on $\Delta^{14}C_{atm}$. (For interpretation of the references to color in this figure, the reader is referred to the web version of this article.)

$\Delta^{14}C_{atm}$ history that generally matches the temporal pattern defined by the $\Delta^{14}C_{atm}$ data (Figs. 5D and 6), without the previously suggested requirement of a severely ^{14}C-deplete stagnant deep ocean carbon reservoir (Broecker and Barker, 2007). As for the Holocene, when the forcing is identical between the "combined deglacial" and "constant Holocene" experiments, the better agreement with observations of the deglacial experiment can be attributed to simulated ^{14}C burial associated with deglacial $CaCO_3$ preservation events that are missing from the "constant Holocene" model scenario.

3.2.3. Thermocline thickness

While the above simulation of combined southern and northern ocean changes can account for major features of the $\Delta^{14}C_{atm}$ history, substantial mismatches remain. In particular, the abrupt $\Delta^{14}C_{atm}$ declines related to NADW re-initiation come too late to capture the rapid $\Delta^{14}C_{atm}$ drops in the latter halves of HS1 and YD, yielding two distinct episodes of model/data divergence (Fig. 5D). The last experiment (Fig. 6) includes a hypothesized thickening of the ocean's main thermocline that draws motivation from physical oceanographic reasoning and helps to address these remaining mismatches.

The rationale of this experiment involves the opposing effects of "northern sinking" (i.e., NADW formation) and wind-driven "southern upwelling" on the depth of the global ocean's main pycnocline (Fig. 4A; Gnanadesikan, 1999). If this logic is applied to the Younger Dryas or any Heinrich Stadial, it calls for global deepening and/or thickening of the ocean's thermocline due to the combination of interrupted "northern sinking" (e.g., McManus et al., 2004) and continued and possibly strengthened "southern upwelling" (due to strengthened and/or southward shifted southern westerly winds; e.g., Anderson et al., 2009; Denton et al., 2010). To explore the sensitivity of $\Delta^{14}C_{atm}$ to thermocline deepening, we use a "thermocline forcing" (Fig. 3F) to mimic the implied circulation changes, superimposed on the "South and North combined" deglacial simulation (Fig. 5D).

The $\Delta^{14}C$ of the "warm upper ocean" above the thermocline is similar to the $\Delta^{14}C$ of the atmosphere, due to ventilation on decadal timescales and a very large gross flux of carbon across the low- and mid-latitude sea surface (Hain et al., 2011). Given a set global inventory of ^{14}C at any given point in time, if the volume of the upper ocean expands at the expense of the volume of the relatively ^{14}C-depleted deep ocean, then the $\Delta^{14}C$ of atmosphere and upper ocean are expected to decline. Indeed, net transfer of ocean volume from the model's deep boxes to the mid-depth boxes (representing the subtropical gyres and the main thermocline) acts to reduce $\Delta^{14}C_{atm}$ by ~13‰ per 100 m simulated deepening of the mid-depth/deep box interface (Fig. 4B). The experiment shown in Fig. 6, which includes a 400 m transient thermocline deepening towards the end of HS1 and YD, transiently reduces simulated $\Delta^{14}C_{atm}$ by up to 50‰ (Fig. 6E) and thereby better matches observed $\Delta^{14}C_{atm}$ during these intervals (Fig. 6D). To be clear, the magnitude and timing of the particular thermocline forcing used in this simulation is chosen to improve the model/data agreement; nevertheless, the underlying physical mechanism is straightforward, and the $\Delta^{14}C_{atm}$ sensitivity is an informative model outcome.

4. Discussion

4.1. Deglacial $\Delta^{14}C_{atm}$ explained?

Given the vigor of the debate regarding the drivers of deglacial $\Delta^{14}C_{atm}$ changes, the model-data fit that we achieve using an idealized deglacial scenario comes as a surprise. It has been argued that only the deglacial release of a hypothesized large and severely ^{14}C-deplete deep ocean carbon reservoir can explain the magnitude and pace of $\Delta^{14}C_{atm}$ decline associated with HS1 (e.g., Broecker and Barker, 2007). Some workers have taken observed $\Delta^{14}C$ anomalies in some mid-depth ocean sites (e.g., Bryan et al., 2010; Marchitto et al., 2007; Thornalley et al., 2011) as support

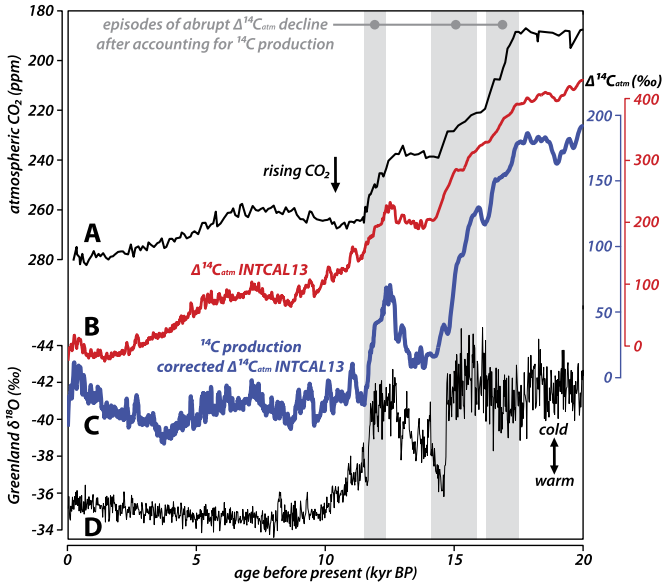

Fig. 7. Illustration of bias introduced by the history of ^{14}C production when comparing $\Delta^{14}C_{atm}$ to atmospheric CO_2. Atmospheric CO_2 (A; Monnin et al., 2001; Lemieux-Dudon et al., 2010) rise across the deglaciation is closely mirrored by declining $\Delta^{14}C_{atm}$ (B; represented here by the central estimate of the INTCAL13 compilation; Reimer et al., 2013). The effect of ^{14}C production changes are accounted for by subtracting from INTCAL13 the median estimate for $\Delta^{14}C_{atm}$ from the "constant Holocene" carbon cycle scenario shown in Fig. 5A. The resulting "^{14}C production corrected INTCAL13" dataset (C) bears some resemblance to both the CO_2 record and climate in Greenland (D; Anderson et al., 2006; NGRIP members 2004; Rasmussen et al., 2006; Vinther et al., 2006). This exercise makes clear that $\Delta^{14}C_{atm}$ is not simply an expression of deglacial CO_2 release from the ocean.

for this assertion, but this line of evidence has a number of shortcomings (e.g., De Pol-Holz et al., 2010; Hain et al., 2011). Similarly, the longstanding argument that deglacial $\Delta^{14}C_{atm}$ decline mirrors deglacial CO_2 rise is not supported by observations when one accounts for the history of ^{14}C production (Fig. 7). Thus, the inference that $\Delta^{14}C_{atm}$ decline was caused by the release of old carbon from the ocean is overly simplistic.

The deglacial simulations presented here demonstrate the plausibility of an alternative "composite" explanation for the $\Delta^{14}C_{atm}$ record that combines Southern Ocean changes with variable North Atlantic circulation and a progressive decline in cosmogenic ^{14}C production. Specifically, based on our simulations, we argue that (1) the decline of the global ^{14}C inventory due to the general decline in ^{14}C production across deglaciation is the single greatest contributor to the deglacial decline of $\Delta^{14}C_{atm}$, (2) the LGM-to-preindustrial contributions to $\Delta^{14}C_{atm}$ decline from Southern Ocean changes that act to release CO_2 and from the deepening of North Atlantic overturning were of similar magnitude, and (3) the repeated stalling and restarting of North Atlantic overturning must leave a distinctive imprint on $\Delta^{14}C_{atm}$. In all deglacial experiments, the ocean's contribution to $\Delta^{14}C_{atm}$ is related to a combination of (a) changes in the ocean's true ventilation age relating to the decay of ^{14}C in the ocean interior, and (b) changes in the ocean's inherited reservoir age resulting from incomplete isotopic equilibration in the surface (e.g., Fig. 6F). In this context, the re-initiation of NADW formation must exert a strong control on $\Delta^{14}C_{atm}$ because it acts to reduce both the ocean's true ventilation age by transporting surface water into the interior and the inherited reservoir age of the interior because North Atlantic ventilated water is relatively well equilibrated with the atmosphere when it descends to depth. These concepts having been enunciated, we acknowledge and further discuss below that the most abrupt reconstructed $\Delta^{14}C_{atm}$ declines precede the consensus timing of the onsets of NADW formation by a few centuries.

4.2. Timing and the role of the thermocline

In our deglacial experiment including both North Atlantic and Southern Ocean changes (Fig. 5D; red in Fig. 6), the simulated $\Delta^{14}C_{atm}$ diverges from reconstructions just prior to both re-initiations of NADW formation at the HS1/Bølling transition and the YD/Holocene transition. This mismatch is critical for the mechanistic interpretation of the $\Delta^{14}C_{atm}$ dataset as a whole, and we entertain three explanations: (1) earlier onset of NADW than is generally believed, (2) error in the reconstructed geomagnetic field strength, and (3) transient deepening of the global thermocline.

The nature of the two episodes of model/data divergence is such that one could say that simulated NADW onsets "come too late" to explain the data. Of course, the timing and/or pace of the forcing could be wrong. Indeed, shifting the onsets of NADW 500 yrs earlier essentially eliminates both episodes of mismatch (results not shown). However, the northward transport, densification and southward return at depth of well ^{14}C-equilibrated and warm low-latitude surface water is the main reason that both $\Delta^{14}C_{atm}$ and circum-North Atlantic climate are highly sensitive to Atlantic overturning. Thus, we tentatively set aside "early NADW" as an explanation based on the well-dated timing of circum-North Atlantic warming, which we take as an indicator of the onsets of NADW formation and its effect on $\Delta^{14}C_{atm}$ (Fig. 6B; but see also Sarnthein et al., 1994; Lynch-Stieglitz et al., 2014, and HS1 data in Thornalley et al., 2011).

Both episodes of model/data divergence coincide with distinctive spikes of low geomagnetic intensity in the GLOPIS-75 dataset, which result in positive spikes of predicted ^{14}C production. There are two main reasons that we suspect that these spikes are artifacts. First, the low magnetic field strength "spikes" tend to populate time intervals of rapid climate change (Fig. 5a), raising the possibility that they are artifacts of sedimentological changes (e.g., Valet, 2003). Second, high-resolution ^{10}Be accumulation in Greenland (Muscheler et al., 2004, 2008) do not support the distinct GLOPIS-75 spikes, at least not on the multi-centennial time-scale implied by the 200-yr sample interval of the GLOPIS dataset. Nevertheless, while these spikes drive a significant portion of the model/data $\Delta^{14}C_{atm}$ divergence, we estimate that not more than about half of the mismatches would be resolved if the ^{14}C production spikes were arbitrarily removed.

Having come to the possibility of deepening of the global thermocline during Heinrich stadials such as YD and HS1, we reiterate that there is physical motivation for it. The lack of NADW/GNAIW formation during these times would have represented a cessation in the removal of buoyant, warm upper ocean water by its conversion to dense deep water. At the same time, net upwelling driven by northward Ekman transport under the southern hemisphere westerly wind belt continued and may have strengthened (Anderson et al., 2009; Toggweiler, 2009; Denton et al., 2010). Thus, during Heinrich stadials, the generation of buoyant upper ocean water by southern westerly-wind driven Ekman transport may have outstripped the loss terms for buoyant water (Toggweiler and Samuels, 1995; Gnanadesikan, 1999; Kuhlbrodt et al., 2007).

In physical models, thermocline deepening is a consequence of "water-hosing" experiments that weaken North Atlantic overturning (e.g., Zhang, 2007; Chang et al., 2008) and of experiments with strengthened southern westerly winds (e.g., Mignone et al., 2006; Lauderdale et al., 2013). The most common parameterization of mesoscale eddies (Gent and McWilliams, 1990) that may balance the purported increase in northward Ekman transport in the Southern Ocean frontal system requires a steepening of the isopycnals, as occurs through thermocline deepening. We estimate, that per 100 m deepening of the thermocline, $\Delta^{14}C_{atm}$ is depressed by 13‰ (Fig. 4B), such that a progressive 400 m deepening of the

global thermocline towards the end of HS1 and the YD could explain the entire model/data mismatch at these times (Fig. 6).

The two episodes of model/data mismatch at the end of HS1 and YD could be a record of physically expected deepening/thickening of the global thermocline, and such thermocline deepening may in turn be fundamental to the physical mechanisms of the bipolar seesaw. With a deepening and/or thickening of the thermocline, the greater volume of buoyant mid-latitude upper ocean water would enhance the meridional sea level gradient (e.g., Stommel, 1961), thereby literally exerting pressure on the North Atlantic to resume NADW formation (Gnanadesikan, 1999; Kuhlbrodt et al., 2007). Thus, evidence for a coherent temporal link between thermocline deepening/thickening and NADW restarts may help to explain the inherent temporal structure of the millennial climate oscillations in the North Atlantic. Previous work invokes an increase in Southern Ocean wind-driven transport as the cause for intensification of Antarctic deep ventilation at the onset of HS1 (Denton et al., 2010). In contrast, we argue that the continued wind-driven upwelling in the Southern Ocean during episodes of stalled NADW formation acts to deepen the global thermocline so as to encourage the re-initiation of deep water formation in the North Atlantic.

4.3. Caveats

The core motivation for this study and the experimental design was to answer a rather straightforward question: How large is the inconsistency between the deglacial $\Delta^{14}C_{atm}$ record and our baseline understanding of ocean changes over this time period? To address this question, we take the GLOPIS-75 record at face value and construct an *ad hoc* deglacial scenario. We emphasize that the simulated $\Delta^{14}C_{atm}$ of this baseline deglacial scenario carries the bias from both the ^{14}C production reconstruction and our implementation of deglacial ocean changes.

Our model predicts a notable increase in $\Delta^{14}C_{atm}$ at the LGM/HS1 transition, in response to the simulated stalling of Atlantic overturning. While there is significant uncertainty in the absolute level of $\Delta^{14}C_{atm}$ (Fig. 1, compare Hulu cave and lake Suigetsu records; Southon et al., 2012; Bronk Ramsey et al., 2012), there is no evidence for a rise in $\Delta^{14}C_{atm}$ at the transition from LGM to HS1. This may indicate that the complete shutdown of North Atlantic-sourced advection in the HS-circulation scheme is too extreme and thus the rise and decline of $\Delta^{14}C_{atm}$ surrounding HS1 and YD are also exaggerated in the model. Similarly, the exact timing of Atlantic circulation changes is only indirectly constrained by Greenland temperature change, and the assumed square-wave pattern is only a crude representation of available reconstructions (e.g., McManus et al., 2004; Lynch-Stieglitz et al., 2011, 2014).

The thermocline mechanism that we invoke to explain the $\Delta^{14}C_{atm}$ decline just prior to NADW re-initiations is speculative and clearly not part of deglacial consensus. However, neither NADW re-initiation nor ocean CO_2 release appear consistent with the timing of the late-HS1 and late-YD model/data deviations. With regard to the record of atmospheric CO_2 concentration, it should be noted that the NADW re-initiations drive simulated short-term CO_2 decline, which are not observed (Figs. 5D and 6). We attribute this mismatch to two factors. First, the simulations are conducted with an isothermal model configuration, and thus the effect of deglacial ocean warming on CO_2 is missing from the simulations (Hain et al., 2010). Second, the response of whole ocean alkalinity in the model may be too slow. The substantial $CaCO_3$ preservation event driven by the NADW onset (Hain et al., 2010) takes thousands of years to manifest. As a result, even though simulated NADW re-initiation raises CO_2 in the steady state, the immediate transient response is a CO_2 decline because it is dominated by the quickly responding effect on the biological pump that lowers CO_2 (e.g., Ito and Follows, 2005; Hain et al., 2010; Sigman et al., 2010; Kwon et al., 2012), without immediate compensation by the solubility pump or whole ocean alkalinity change. These deficiencies with regard to simulated CO_2 have no significant bearing on simulated $\Delta^{14}C_{atm}$, which is driven by isotopic equilibration via gross (not net) gas-exchange in the surface along with changes in the true (ideal) ventilation age of the ocean interior.

5. Conclusion

We present the most rigorous attempt to date to simulate the deglacial history of atmospheric $\Delta^{14}C$ changes, accounting for the effect of changes in Earth's magnetic field strength (and its uncertainty) on cosmogenic ^{14}C production and separating the contributions of changes in the North Atlantic and Southern Oceans. Our simulations suggest that the repeated stalling and resumption of NADW formation was the principle driver for the two main deglacial episodes of rapid $\Delta^{14}C_{atm}$ decline, with much of the effect related to the high degree of $\Delta^{14}C$ equilibration of northern-sourced deep waters. That is, $\Delta^{14}C_{atm}$ is highly sensitive to deep water formation in the North Atlantic because it drives changes in both the true (ideal) ventilation age and the reservoir effect inherited by the global deep ocean. Southern Ocean changes that dominate CO_2 release from the deep ice age ocean cause only modest $\Delta^{14}C_{atm}$ decline because the Southern Ocean surface is poorly equilibrated with respect to atmospheric $\Delta^{14}C$. If this "composite" view of the deglacial $\Delta^{14}C_{atm}$ record is accepted, the onset of $\Delta^{14}C_{atm}$ decline ~5 centuries prior to the onsets of NADW formation requires an additional, as yet unrecognized process. We propose that the "early" $\Delta^{14}C_{atm}$ decline is the signature of the deepening/thickening of the global thermocline, driven by northward Ekman transport under the southern westerly wind belt in the absence of NADW formation. This interpretation implies a role for the southern westerly winds in restarting NADW formation.

Acknowledgements

The authors thank C. Laj and I. Usoskin for sharing the GLOPIS dataset and the ^{14}C production model, and E. Bard, M. Bender, W. Broecker, J. Sarmiento and S. Thornalley for discussion. Reviews by the editor J. Lynch-Stieglitz, J. Adkins, and an anonymous reviewer greatly improved the manuscript. Support was provided by the Walbridge Fund Graduate Award of the Princeton Environmental Institute, the Charlotte Elizabeth Procter Honorific Fellowship of Princeton University (to M.P.H.), the UK NERC Grant NE/K00901X/1 (to M.P.H), the US NSF Grant OCE1234664 (to D.M.S.), the German DFG (Gottfried Wilhelm Leibniz Award to G.H.H.), the Alexander von Humboldt Foundation through the Friedrich Wilhelm Bessel Award (to D.M.S.) and the John D. and Catherine T. MacArthur Foundation through its Fellows Program (to D.M.S.).

Appendix A. Supplementary material

Supplementary material related to this article can be found online at http://dx.doi.org/10.1016/j.epsl.2014.03.020.

References

Andersen, K.K., Svensson, A., Johnsen, S.J., Rasmussen, S.O., Bigler, M., Rothlisberger, R., Ruth, U., Siggaard-Andersen, M.-L., Steffensen, J.P., Dahl-Jensen, D., Vinther, B.M., Clausen, H.B., 2006. The Greenland ice core chronology 2005, 15–42 ka. Part 1: constructing the time scale. Quat. Sci. Rev. 25, 3246–3257.

Anderson, R.F., Ali, S., Bradtmiller, L.I., Nielsen, S.H.H., Fleisher, M.Q., Anderson, B.E., Burckle, L.H., 2009. Wind-driven upwelling in the Southern Ocean and the deglacial rise in atmospheric CO_2. Science 323, 1443–1448.

Andresen, C.S., Björck, S., Bennike, O., Heinemeier, J., Kromer, B., 2000. What do $\Delta^{14}C$ changes across the Gerzensee oscillation/GI-1b event imply for deglacial oscillations?. J. Quat. Sci. 15 (3), 203–214.

Archer, D., 1991. Modeling the calcite lysocline. J. Geophys. Res., Oceans 96, 17037–17050.

Bard, E., 1998. Geochemical and geophysical implications of the radiocarbon calibration. Geochim. Cosmochim. Acta 62, 2025–2038.

Blunier, T., Brook, E.J., 2001. Timing of millennial-scale climate change in Antarctica and Greenland during the last glacial period. Science 291, 109–112.

Broecker, W., Barker, S., 2007. A 190% drop in atmosphere's $\Delta^{14}C$ during the "Mystery Interval" (17.5 to 14.5 kyr). Earth Planet. Sci. Lett. 256, 90–99.

Broecker, W.S., 2009. The mysterious ^{14}C decline. Radiocarbon 51, 109–119.

Bronk Ramsey, C.B., Staff, R.A., Bryant, C.L., Brock, F., Kitagawa, H., van der Plicht, J., Schlolaut, G., Marshall, M.H., Brauer, A., Lamb, H.F., Payne, R.L., Tarasov, P.E., Haraguchi, T., Gotanda, K., Yonenobu, H., Yokoyama, Y., Tada, R., Nakagawa, T., 2012. A complete terrestrial radiocarbon record for 11.2 to 52.8 kyr BP. Science 338, 370–374.

Bryan, S.P., Marchitto, T.M., Lehman, S.J., 2010. The release of ^{14}C-depleted carbon from the deep ocean during the last deglaciation: evidence from the Arabian Sea. Earth Planet. Sci. Lett. 298, 244–254.

Chang, P., Zhang, R., Hazeleger, W., Wen, C., Wan, X.Q., Ji, L., Haarsma, R.J., Breugem, W.P., Seidel, H., 2008. Oceanic link between abrupt changes in the North Atlantic Ocean and the African monsoon. Nat. Geosci. 1, 444–448.

Collins, L.G., Pike, J., Allen, C.S., Hodgson, D.A., 2012. High-resolution reconstruction of southwest Atlantic sea–ice and its role in the carbon cycle during marine isotope stages 3 and 2. Paleoceanography 27.

Curry, W.B., Oppo, D.W., 2005. Glacial water mass geometry and the distribution of $\delta^{13}C$ of $\sum CO_2$ in the western Atlantic Ocean. Paleoceanography 20.

De Pol-Holz, R., Keigwin, L., Southon, J., Hebbeln, D., Mohtadi, M., 2010. No signature of abyssal carbon in intermediate waters off Chile during deglaciation. Nat. Geosci. 3, 192–195.

Denton, G.H., Anderson, R.F., Toggweiler, J.R., Edwards, R.L., Schaefer, J.M., Putnam, A.E., 2010. The last glacial termination. Science 328, 1652–1656.

Donnelly, J.P., Driscoll, N.W., Uchupi, E., Keigwin, L.D., Schwab, W.C., Thieler, E.R., Swift, S.A., 2005. Catastrophic meltwater discharge down the Hudson Valley: a potential trigger for the Intra-Allerod cold period. Geology 33, 89–92.

Duplessy, J.C., Shackleton, N.J., Fairbanks, R.G., Labeyrie, L., Oppo, D., Kallel, N., 1988. Deepwater source variations during the last climatic cycle and their impact on the global deepwater circulation. Paleoceanography 3, 343–360.

Eicher, U., Siegenthaler, U., 1976. Palynological and oxygen isotope investigations on glacial sediment cores from Swiss lakes. Boreas 5, 109–117.

François, R., Altabet, M.A., Yu, E.F., Sigman, D.M., Bacon, M.P., Frank, M., Bohrmann, G., Bareille, G., Labeyrie, L.D., 1997. Contribution of Southern Ocean surface-water stratification to low atmospheric CO_2 concentrations during the last glacial period. Nature 389, 929–935.

Friedrich, M., Remmelel, S., Kromer, B., Hofmann, J., Spurk, M., Kaiser, K.F., Orcel, C., Kuppers, M., 2004. The 12,460-year Hohenheim oak and pine tree-ring chronology from central Europe – a unique annual record for radiocarbon calibration and paleoenvironment reconstructions. Radiocarbon 46, 1111–1122.

Gent, P., McWilliams, J., 1990. Isopycnal mixing in ocean circulation models. J. Phys. Oceanogr. 20, 150–155.

Gnanadesikan, A., 1999. A simple predictive model for the structure of the oceanic pycnocline. Science 283, 2077–2079.

Hain, M.P., Sigman, D.M., Haug, G.H., 2010. Carbon dioxide effects of Antarctic stratification, North Atlantic Intermediate Water formation, and subantarctic nutrient drawdown during the last ice age: diagnosis and synthesis in a geochemical box model. Glob. Biogeochem. Cycles 24.

Hain, M.P., Sigman, D.M., Haug, G.H., 2011. Shortcomings of the isolated abyssal reservoir model for deglacial radiocarbon changes in the mid-depth Indo-Pacific Ocean. Geophys. Res. Lett. 38.

Hain, M.P., Sigman, D.M., Haug, G.H., 2014. The biological pump in the past. In: Holland, Heinrich D., Turekian, Karl K. (Eds.), Treatise in Geochemistry. 2nd ed. Elsevier, Oxford, ISBN 978-0-08-098300-4, pp. 485–517.

Hughen, K., Lehman, S., Southon, J., Overpeck, J., Marchal, O., Herring, C., Turnbull, J., 2004. ^{14}C activity and global carbon cycle changes over the past 50,000 years. Science 303, 202–207.

Hughen, K.A., Overpeck, J.T., Lehman, S.J., Kashgarian, M., Southon, J., Peterson, L.C., Alley, R., Sigman, D.M., 1998. Deglacial changes in ocean circulation from an extended radiocarbon calibration. Nature 391, 65–68.

Ito, T., Follows, M.J., 2005. Preformed phosphate, soft tissue pump and atmospheric CO_2. J. Mar. Res. 63, 813–839.

Jouzel, J., Masson-Delmotte, V., Cattani, O., Dreyfus, G., Falourd, S., Hoffmann, G., Minster, B., Nouet, J., Barnola, J.M., Chappellaz, J., Fischer, H., Gallet, J.C., Johnsen, S., Leuenberger, M., Loulergue, L., Luethi, D., Oerter, H., Parrenin, F., Raisbeck, G., Raynaud, D., Schilt, A., Schwander, J., Selmo, E., Souchez, R., Spahni, R., Stauffer, B., Steffensen, J.P., Stenni, B., Stocker, T.F., Tison, J.L., Werner, M., Wolff, E.W., 2007. Orbital and millennial Antarctic climate variability over the past 800,000 years. Science 317, 793–796.

Keir, R.S., 1983. Reduction of the thermohaline circulation during deglaciation – the effect on atmospheric radiocarbon and CO_2. Earth Planet. Sci. Lett. 64, 445–456.

Keir, R.S., 1988. On the Late Pleistocene ocean geochemistry and circulation. Paleoceanography 3, 413–445.

Kohfeld, K.E., Le Quere, C., Harrison, S.P., Anderson, R.F., 2005. Role of marine biology in glacial–interglacial CO_2 cycles. Science 308, 74–78.

Köhler, P., Muscheler, R., Fischer, H., 2006. A model-based interpretation of low-frequency changes in the carbon cycle during the last 120,000 years and its implications for the reconstruction of atmospheric $\Delta^{14}C$. Geochem. Geophys. Geosyst. 7.

Kovaltsov, G.A., Mishev, A., Usoskin, I.G., 2012. A new model of cosmogenic production of radiocarbon ^{14}C in the atmosphere. Earth Planet. Sci. Lett. 337, 114–120.

Kuhlbrodt, T., Griesel, A., Montoya, M., Levermann, A., Hofmann, M., Rahmstorf, S., 2007. On the driving processes of the Atlantic meridional overturning circulation. Rev. Geophys. 45. http://dx.doi.org/10.1029/2004RG000166.

Kumar, N., Anderson, R.F., Mortlock, R.A., Froelich, P.N., Kubik, P., Dittrichhannen, B., Suter, M., 1995. Increased biological productivity and export production in the glacial Southern-Ocean. Nature 378, 675–680.

Kwon, E.Y., Hain, M.P., Sigman, D.M., Galbraith, E.D., Sarmiento, J.L., Toggweiler, J.R., 2012. North Atlantic ventilation of "southern-sourced" deep water in the glacial ocean. Paleoceanography 27.

Kwon, E.Y., Sarmiento, J.L., Toggweiler, J.R., DeVries, T., 2011. The control of atmospheric pCO_2 by ocean ventilation change: the effect of the oceanic storage of biogenic carbon. Glob. Biogeochem. Cycles 25.

Laj, C., Kissel, C., Beer, J., 2004. High resolution global paleointensity stack since 75 kyr (GLOPIS-75) calibrated to absolute values. In: Geophysical Monograph Series, vol. 145, pp. 255–265.

Laj, C., Kissel, C., Mazaud, A., Michel, E., Muscheler, R., Beer, J., 2002. Geomagnetic field intensity, North Atlantic Deep Water circulation and atmospheric $\Delta^{14}C$ during the last 50 kyr. Earth Planet. Sci. Lett. 200, 177–190.

Lal, D., Peters, B., 1967. Cosmic rays produced radioactivity on the Earth. In: Handbuch der Physik, vol. 46, pp. 551–612.

Lauderdale, J.M., Garabato, A.C.N., Oliver, K.I.C., Follows, M.J., Williams, R.G., 2013. Wind-driven changes in Southern Ocean residual circulation, ocean carbon reservoirs and atmospheric CO_2. Clim. Dyn. 41, 2145–2164.

Lehman, S.J., Keigwin, L.D., 1992. Sudden changes in North-Atlantic circulation during the last deglaciation. Nature 356, 757–762.

Lemieux-Dudon, B., Blayo, E., Petit, J.-R., Waelbroeck, C., Svensson, A., Ritz, C., Barnola, J.-M., Narcisi, B.M., Parrenin, F., 2010. Consistent dating for Antarctic and Greenland ice cores. Quat. Sci. Rev. 29, 8–20.

Levesque, A.J., Mayle, F.E., Walker, I.R., Cwynar, L.C., 1993. A previously unrecognized late-glacial cold event in eastern North-America. Nature 361, 623–626.

Lippold, J., Luo, Y., Francois, R., Allen, S.E., Gherardi, J., Pichat, S., Hickey, B., Schulz, H., 2012. Strength and geometry of the glacial Atlantic Meridional Overturning Circulation. Nat. Geosci. 5, 813–816.

Lynch-Stieglitz, J., Adkins, J.F., Curry, W.B., Dokken, T., Hall, I.R., Herguera, J.C., Hirschi, J.J.M., Ivanova, E.V., Kissel, C., Marchal, O., Marchitto, T.M., McCave, I.N., McManus, J.F., Mulitza, S., Ninnemann, U., Peeters, F., Yu, E.-F., Zahn, R., 2007. Atlantic meridional overturning circulation during the Last Glacial Maximum. Science 316, 66–69.

Lynch-Stieglitz, J., Schmidt, M.W., Curry, W.B., 2011. Evidence from the Florida Straights for Younger Dryas ocean circulation changes. Paleoceanography 26, PA1205. http://dx.doi.org/10.1029/2010PA002332.

Lynch-Stieglitz, J., Schmidt, M.W., Henry, L.G., Curry, W.B., Skinner, L.C., Mulitza, S., Zhang, R., Chang, P., 2014. Muted change in Atlantic overturning circulation over some glacial-aged Heinrich events. Nat. Geosci. 7. http://dx.doi.org/10.1038/ngeo2045.

Lynch-Stieglitz, J., Stocker, T.F., Broecker, W.S., Fairbanks, R.G., 1995. The influence of air–sea exchange on the isotopic composition of oceanic carbon – observations and modeling. Glob. Biogeochem. Cycles 9, 653–665.

Marchitto, T.M., Broecker, W.S., 2006. Deep water mass geometry in the glacial Atlantic Ocean: a review of constraints from the paleonutrient proxy Cd/Ca. Geochem. Geophys. Geosyst. 7.

Marchitto, T.M., Curry, W.B., Oppo, D.W., 1998. Millennial-scale changes in North Atlantic circulation since the last glaciation. Nature 393, 557–561.

Marchitto, T.M., Lehman, S.J., Ortiz, J.D., Fluckiger, J., van Geen, A., 2007. Marine radiocarbon evidence for the mechanism of deglacial atmospheric CO_2 rise. Science 316, 1456–1459. http://dx.doi.org/10.1126/science.1138679.

Martin, J.H., 1990. Glacial–interglacial CO_2 change: The iron hypothesis. Paleoceanography 5, 1–13.

Martinez-Garcia, A., Rosell-Mele, A., Geibert, W., Gersonde, R., Masque, P., Gaspari, V., Barbante, C., 2009. Links between iron supply, marine productivity, sea surface temperature, and CO_2 over the last 1.1 Ma. Paleoceanography 24.

Martinez-Garcia, A., Sigman, D.M., Ren, H., Anderson, R.F., Straub, M., Hodell, D.A., Jaccard, S.L., Eglinton, T.I., Haug, G.H., 2014. Iron fertilization of the Subantarctic ocean during the last ice age. Science 343 (6177), 1347–1350. http://dx.doi.org/10.1126/science.1246848.

Masarik, J., Beer, J., 1999. Simulation of particle fluxes and cosmogenic nuclide production in the Earth's atmosphere. J. Geophys. Res., Atmos. 104, 12099–12111.

Masarik, J., Beer, J., 2009. An updated simulation of particle fluxes and cosmogenic nuclide production in the Earth's atmosphere. J. Geophys. Res., Atmos. 114, 9.

Matsumoto, K., Yokoyama, Y., 2013. Atmospheric ^{14}C reduction in simulations of Atlantic overturning circulation shutdown. Global Biogeochem. Cycles 27. http://dx.doi.org/10.1002/gbc.20035.

McManus, J.F., Francois, R., Gherardi, J.M., Keigwin, L.D., Brown-Leger, S., 2004. Collapse and rapid resumption of Atlantic meridional circulation linked to deglacial climate changes. Nature 428, 834–837.

NGRIP members, 2004. High-resolution record of Northern Hemisphere climate extending into the last interglacial period. Nature 431, 147–151.

Mignone, B.K., Gnanadesikan, A., Sarmiento, J.L., Slater, R.D., 2006. Central role of Southern Hemisphere winds and eddies in modulating the oceanic uptake of anthropogenic carbon. Geophys. Res. Lett. 33, 5.

Monnin, E., Indermuhle, A., Dallenbach, A., Fluckiger, J., Stauffer, B., Stocker, T.F., Raynaud, D., Barnola, J.M., 2001. Atmospheric CO_2 concentrations over the last glacial termination. Science 291, 112–114.

Muscheler, R., Beer, J., Wagner, G., Laj, C., Kissel, C., Raisbeck, G.M., Yiou, F., Kubik, P.W., 2004. Changes in the carbon cycle during the last deglaciation as indicated by the comparison of ^{10}Be and ^{14}C records. Earth Planet. Sci. Lett. 219, 325–340.

Muscheler, R., Kromer, B., Bjorck, S., Svensson, A., Friedrich, M., Kaiser, K.F., Southon, J., 2008. Tree rings and ice cores reveal ^{14}C calibration uncertainties during the Younger Dryas. Nat. Geosci. 1, 263–267.

Rasmussen, S.O., Andersen, K.K., Svensson, A.M., Steffensen, J.P., Vinther, B.M., Clausen, H.B., Siggaard-Andersen, M.L., Johnsen, S.J., Larsen, L.B., Dahl-Jensen, D., Bigler, M., Rothlisberger, R., Fischer, H., Goto-Azuma, K., Hansson, M.E., Ruth, U., 2006. A new Greenland ice core chronology for the last glacial termination. J. Geophys. Res., Atmos. 111.

Reimer, P.J., et al., 2013. IntCal13 and Marine13 radiocarbon age calibration curves 0–50,000 years cal BP. Radiocarbon 55, 1869–1887.

Reimer, P.J., Baillie, M.G.L., Bard, E., Bayliss, A., Beck, J.W., Bertrand, C.J.H., Blackwell, P.G., Buck, C.E., Burr, G.S., Cutler, K.B., Damon, P.E., Edwards, R.L., Fairbanks, R.G., Friedrich, M., Guilderson, T.P., Hogg, A.G., Hughen, K.A., Kromer, B., McCormac, G., Manning, S., Ramsey, C.B., Reimer, R.W., Remmele, S., Southon, J.R., Stuiver, M., Talamo, S., Taylor, F.W., van der Plicht, J., Weyhenmeyer, C.E., 2004. IntCal04 terrestrial radiocarbon age calibration, 0–26 cal kyr BP. Radiocarbon 46, 1029–1058.

Reimer, P.J., Baillie, M.G.L., Bard, E., Bayliss, A., Beck, J.W., Blackwell, P.G., Ramsey, C.B., Buck, C.E., Burr, G.S., Edwards, R.L., Friedrich, M., Grootes, P.M., Guilderson, T.P., Hajdas, I., Heaton, T.J., Hogg, A.G., Hughen, K.A., Kaiser, K.F., Kromer, B., McCormac, F.G., Manning, S.W., Reimer, R.W., Richards, D.A., Southon, J.R., Talamo, S., Turney, C.S.M., van der Plicht, J., Weyhenmeye, C.E., 2009. INTCAL09 and MARINE09 radiocarbon age calibration curves, 0–50,000 years CAL BP. Radiocarbon 51, 1111–1150.

Ritz, S.P., Stocker, T.F., Grimalt, J.O., Menviel, L., Timmermann, A., 2013. Estimated strength of the Atlantic overturning circulation during the last deglaciation. Nat. Geosci. 6, 208–212.

Robinson, L.F., Adkins, J.F., Keigwin, L.D., Southon, J., Fernandez, D.P., Wang, S.L., Scheirer, D.S., 2005a. Radiocarbon variability in the western North Atlantic during the last deglaciation. Science 310, 1469–1473.

Robinson, R.S., Brunelle, B.G., Sigman, D.M., 2004. Revisiting nutrient utilization in the glacial Antarctic: evidence from a new method for diatom-bound N isotopic analysis. Paleoceanography 19.

Robinson, R.S., Sigman, D.M., 2008. Nitrogen isotopic evidence for a poleward decrease in surface nitrate within the ice age Antarctic. Quat. Sci. Rev. 27, 1076–1090.

Robinson, R.S., Sigman, D.M., DiFiore, P.J., Rohde, M.M., Mashiotta, T.A., Lea, D.W., 2005b. Diatom-bound ^{15}N/^{14}N: New support for enhanced nutrient consumption in the ice age subantarctic. Paleoceanography 20.

Sarnthein, M., Winn, K., Jung, S.J.A., Duplessy, J.C., Labeyrie, L., Erlenkeuser, H., Ganssen, G., 1994. Changes in east Atlantic deep-water circulation over the last 30,000 years – 8 time slice reconstructions. Paleoceanography 9, 209–267.

Southon, J., Noronha, A.L., Cheng, H., Edwards, R.L., Wang, Y.J., 2012. A high-resolution record of atmospheric ^{14}C based on Hulu Cave speleothem H82. Quat. Sci. Rev. 33, 32–41.

Siani, G., Michel, E., De Pol-Holz, R., DeVries, T., Lamy, F., Carel, M., Isguder, G., Dewilde, F., Lourantou, A., 2013. Carbon isotope records reveal precise timing of enhanced Southern Ocean upwelling during the last deglaciation. Nat. Commun. 4. http://dx.doi.org/10.1038/ncomms3758.

Sigman, D.M., Hain, M.P., Haug, G.H., 2010. The polar ocean and glacial cycles in atmospheric CO_2 concentration. Nature 466, 47–55.

Sigman, D.M., Lehman, S.J., Oppo, D.W., 2003. Evaluating mechanisms of nutrient depletion and ^{13}C enrichment in the intermediate-depth Atlantic during the last ice age. Paleoceanography 18.

Sigman, D.M., McCorkle, D.C., Martin, W.R., 1998. The calcite lysocline as a constraint on glacial/interglacial low-latitude production changes. Glob. Biogeochem. Cycles 12, 409–427.

Skinner, L.C., Fallon, S., Waelbroeck, C., Michel, E., Barker, S., 2010. Ventilation of the deep southern ocean and deglacial CO_2 rise. Science 328, 1147–1151.

Stephens, B.B., Keeling, R.F., 2000. The influence of Antarctic sea ice on glacial–interglacial CO_2 variations. Nature 404, 171–174.

Stommel, H., 1961. Thermohaline convection with two stable regimes of flow. Tellus 13, 224–230.

Thornalley, D.J.R., Barker, S., Broecker, W.S., Elderfield, H., McCave, I.N., 2011. The deglacial evolution of North Atlantic deep convection. Science 331, 202–205.

Toggweiler, J.R., 2009. Shifting westerlies. Science 323, 1434–1435.

Toggweiler, J.R., Samuels, B., 1995. Effect of Drake Passage on the global thermohaline circulation. Deep-Sea Res., Part 1, Oceanogr. Res. Pap. 42, 477–500.

Valet, J.P., 2003. Time variations in geomagnetic intensity. Rev. Geophys. 41, 44.

van Raden, Ulrike J., Colombaroli, Daniele, Gilli, Adrian, Schwander, Jakob, Bernasconi, Stefano M., van Leeuwen, Jacqueline, Leuenberger, Markus, Eicher, Ueli, 2013. High-resolution late-glacial chronology for the Gerzensee lake record (Switzerland): δ^{18}O correlation between a Gerzensee-stack and NGRIP. Palaeogeogr. Palaeoclimatol. Palaeoecol. 391, Part B (ISSN 0031-0182), 13–24. http://dx.doi.org/10.1016/j.palaeo.2012.05.017.

Vinther, B.M., Clausen, H.B., Johnsen, S.J., Rasmussen, S.O., Andersen, K.K., Buchardt, S.L., Dahl-Jensen, D., Seierstad, I.K., Siggaard-Andersen, M.L., Steffensen, J.P., Svensson, A., Olsen, J., Heinemeier, J., 2006. A synchronized dating of three Greenland ice cores throughout the Holocene. J. Geophys. Res., Atmos. 111.

Wang, Y.J., Cheng, H., Edwards, R.L., An, Z.S., Wu, J.Y., Shen, C.C., Dorale, J.A., 2001. A high-resolution absolute-dated Late Pleistocene monsoon record from Hulu Cave, China. Science 294, 2345–2348.

Zhang, R., 2007. Anticorrelated multidecadal variations between surface and subsurface tropical North Atlantic. Geophys. Res. Lett. 34, 6.